

## Early Archean alteration minerals in mafic-ultramafic rocks of the Barberton greenstone belt as petrological analogs for clay mineralogy on Mars

EUGENE G. GROSCH<sup>1,\*</sup>†, JANICE L. BISHOP<sup>2</sup>, CHRISTIAN MIELKE<sup>3</sup>, ALESSANDRO MATURILLI<sup>4</sup>, AND JÖRN HELBERT<sup>4</sup>

<sup>1</sup>Geology Department, Rhodes University, Grahamstown/Makhanda 6140, South Africa

<sup>2</sup>Carl Sagan Center, SETI Institute and NASA-Ames Research Center, Mountain View, California 94043, U.S.A.

<sup>3</sup>GFZ German Research Centre for Geosciences, Telegrafenberg, 14473 Potsdam

<sup>4</sup>Institute for Planetary Research, DLR, Rutherfordstrasse 2, 12489, Berlin-Adlershof, Germany,

### ABSTRACT

Characterization of terrestrial analog sites is critical for detection and determination of clay mineralogy in remote sensing studies of Mars aimed at geological, hydrological, and potentially biological investigations. In this study, we investigate a suite of hydrothermally altered early Archean rocks from the Barberton greenstone belt (BGB) of South Africa as potential petrological, mineralogical, and spectral analogs to hydrothermally altered metabasalts and mafic-ultramafic intrusions in the martian subsurface and impact craters. We present the first spectral imaging measurements on exceptionally well-preserved early Archean mafic-ultramafic rocks from the BGB, with the aim of studying their clay mineralogy and spectral signatures. Multiple spectral analyses were conducted on different sample textures (rock powders, crushed rocks, and rock slabs) appropriate for Mars rover and remote sensing exploration. Visible/near-infrared (VNIR) and mid-IR reflectance spectra were acquired on particulate samples, while VNIR spectral imaging data were collected on rock slabs. Mid-IR emission spectra were measured for the rock slabs and grains. Spectral features are compared from these different spectral techniques to identify the minerals present in the samples and compare macroscale vs. microscale detections. The measured spectra reveal absorption bands that correspond to clay mineralogy of the serpentine and chlorite mineral groups, consistent with petrographic observations, as well as magnetite, olivine, quartz, feldspar, and Al-phyllsilicate. The spectral data acquired in this study expand the reference spectra data set for remote sensing studies. The implications of this study are that rocks from early Archean greenstone belts, such as those of the BGB, serve as potential clay-bearing petrological analogs for hydrothermal environments on Mars.

**Keywords:** Barberton greenstone belt, early Earth, Archean metabasalts, Mars petrological analogs; Earth Analogs for Martian Geological Materials and Processes

### INTRODUCTION

In the search for life on Mars, “follow the water” has been a validated and useful approach. The main indicator of surface and subsurface groundwater on Mars is the presence of low-temperature alteration minerals such as phyllosilicates, opal, zeolite, and sulfate (e.g., Murchie et al. 2019; Carter et al. 2013; Ehlmann and Edwards 2014). Orbital remote sensing missions and Mars rover observations have found evidence for alteration and clay formation in multiple surface and subsurface environments, including various hydrothermal conditions (e.g., Ehlmann et al. 2009, 2010, 2011a, 2013; Marzo et al. 2010; Squyres et al. 2012; Bishop et al. 2013; Michalski et al. 2013, 2017; Bridges et al. 2015; Bristow et al. 2015). These studies report in situ and hyperspectral data in support of the relatively common occurrence of (Fe,Mg)-rich phyllosilicates (e.g., smectite, chlorite, and serpentine) and Al-rich phyllosilicates (kaolinite, montmorillonite) on the exposed surface of Mars. Lab spectra of clay-bearing rocks from various hydrothermal settings on Earth (e.g., Bishop

et al. 2002, 2004, 2007; Michalski et al. 2006; Schiffman et al. 2006; Hamilton et al. 2008; Ehlmann et al. 2011b, 2012; Cuadros et al. 2013; Yant et al. 2018) provide important constraints on geochemical conditions, temperature, type of salts, and nature of water activity on Mars. Furthermore, sub-surface mafic-ultramafic hydrothermal environments on early Earth and Mars may have been very similar (e.g., Cockell 2006; Izawa et al. 2019; Grosch and Hazen 2015). Investigation of Fe/Mg-rich clays from seafloor sites (Cuadros et al. 2013) has led to characterization of distinct types of clays on Mars (Michalski et al. 2015; Bishop et al. 2018). Consequently, clay-bearing early Archean terrestrial rocks may be useful as analog materials to extend the visible/near-infrared (VNIR) and mid-infrared (mid-IR) spectral databases for remote sensing studies on orbital and rover missions at Mars. It is important to point out that clay mineral formation processes on early Earth and Mars may not necessarily have been the same in all geological environments, and we propose that the Barberton rocks are possible petrological analogs, not necessarily direct alteration process analogs. However, the early sub-surface hydrothermal environments may have been similar in some parts of early Earth and Mars.

Bioalteration of basaltic volcanic glass is a model that has

\* E-mail: geogene@gmail.com

† Special collection papers can be found online at <http://www.minsocam.org/MSA/AmMin/special-collections.html>.

been invoked to explain the occurrence of granular and tubular microstructures in modern and ancient volcanic glass (Thorseth et al. 1995; Fisk et al. 1998; Furnes et al. 2001). In this model, chemolithoautotrophic microorganisms are believed to be involved in accelerating glass dissolution for nutrients and energy-producing microborings (e.g., Thorseth et al. 1995). In the modern oceanic crust, the existence of a subsurface biosphere is supported by a range of evidence that includes microbiological data, sulfur and carbon isotopes, and detailed reviews of this body of evidence can be found in Orcutt et al. (2011), Edward et al. (2011), and Thorseth (2011). Titanite microstructures in ophiolite and Archean pillow lavas have also been argued to represent early microborings by microorganisms thriving in the Archean subsurface environment (Furnes et al. 2004; Banerjee et al. 2007; Staudigel et al. 2008), although the biogenicity and syngeneticity of these structures have been brought into question by Grosch and McLoughlin (2014). However, it is not impossible that the oceanic hydrothermal subsurface was a habitat for the earliest microbial life protected from harsh UV rays on early Earth. This has important astrobiological implications as it would suggest that early mafic-ultramafic hydrothermal subsurface environments beneath martian impact craters may have been favorable sites for microbial life to thrive (e.g., Cockell 2006). As a hypothesis, the hydrothermal mafic-ultramafic subsurface environments on early Earth and early Mars may both have been potentially habitable sites, particularly given the evidence for water on early Mars (e.g., Craddock and Howard 2002; Cockell 2006; Grosch and Hazen 2015; Izawa et al. 2019).

The 3.55 to 3.10 billion year old rocks of the early Archean Barberton greenstone belt (BGB) volcano-sedimentary succession represent an exceptionally well-preserved rock archive of early Earth processes. In this study, we make the case that altered, silicified, serpentinized, and clay-bearing mafic-ultramafic rock samples from the early Archean BGB may prove to be useful petrological analogs for low-temperature martian environments. Hydrogen production from low-temperature alteration of ultramafic and basaltic rocks has been proposed to support early microbial life in Earth's earliest subsurface environments, which may have been the case for early Mars (Oze and Sharma 2005; Grosch and Hazen 2015). Investigation of serpentines on Mars has also received attention as a potential source of H<sub>2</sub> and methane that could have supported microbial life (Ehlmann et al. 2010; Mustard and Tarnas 2017). Archean terrestrial rock environments preserved in greenstone belts may play an important role in understanding early martian subsurface environments relevant to the search for extraterrestrial life and water. Previous studies have successfully provided hyperspectral maps of altered, clay-bearing outcrops in the early Archean North Pole Dome of the Pilbara Craton (Brown et al. 2004, 2007). In this context, the rock sequences of the Paleoproterozoic BGB of South Africa provide unique martian analogs as these rocks are exceptionally well preserved and record early Earth surface and subsurface processes that could be related to processes on early Mars as well. Geological evidence for early Archean sedimentary  $\delta$  fan deposits (Drabon et al. 2019), storm-reworked volcanic deposits (Trower and Lowe 2016), and spherule beds marking violent meteorite impacts (Lowe et al. 2003, 2014) have all been reported from the Barberton greenstone belt. In situ exploration by rovers, remote

sensing studies, and meteorite evidence has indicated the presence of metabasalts, altered gabbros, olivine-/pyroxene-bearing basalts, serpentinized picritic basalts, or peridotites on Mars.

In this study we present spectra of several 3.4 to 3.5 billion year old Archean mafic-ultramafic greenstone belt rock samples as analog materials that include chloritized and silicified tholeiitic basalts, basaltic komatiites, serpentinized ultramafic komatiites, and a felsic tonalite (see Table 1). These Archean BGB samples were characterized petrologically in previous studies (e.g., Grosch et al. 2012; Bost et al. 2013). The field setting on an outcrop scale, petrography, and mineralogy of the Archean BGB samples are presented here. Mineral composition data on relic igneous and clay mineral phases are discussed in context with the spectroscopy results. We have analyzed VNIR and mid-IR reflectance spectra and mid-IR emission spectra on these early Archean samples with the aim of using these spectra for ground-truthing remote sensing data and performing mineral identification and characterization of alteration environments on Mars. Specifically, the VNIR spectra cover the spectral range collected by Compact Reconnaissance Imaging Spectrometer for Mars (CRISM) (Murchie et al. 2019) on the Mars Reconnaissance Orbiter (MRO) and the MicrOmega instrument (Bibring et al. 2017) planned for ESA's ExoMars rover. The mid-IR spectra cover the spectral range measured by Thermal Emission Spectrometer (TES) (Christensen et al. 2001) on the Mars Global Surveyor orbiter as well as the Mini-TES spectrometer on board the Mars Exploration (MER) rovers (e.g., Christensen et al. 2003; Ruff et al. 2019). VNIR reflectance spectra acquired of individual rock surfaces and size fractions are compared to VNIR reflectance imaging of rock surfaces. This study provides an opportunity to evaluate alteration on ancient Earth rocks and provides spectral data sets to search for related phyllosilicates and hydrous minerals on Mars.

### BARBERTON EARLY EARTH ANALOG SITES FOR MARS

The Paleoproterozoic BGB hosts some of the world's best-preserved rocks of the early Archean eon and some of the earliest traces of microbial life preserved in shallow silicified seafloor sediments, known as cherts (Walsh 1992) and potentially in volcanic subsurface environments (McLoughlin et al. 2012 and references therein). Exceptionally well-preserved tectonic slivers of altered Mesoproterozoic oceanic crust and associated sediments have been identified, providing a unique mineralogical and petrological archive of information related to the evolution of early Earth (Grosch et al. 2012). For these reasons, the early Archean BGB rocks have been at the center of several international scientific drilling projects (e.g., Grosch et al. 2009; Philippot et al. 2009).

This study focuses on rocks from the 3.55 to 3.33 Ga Onverwacht Group of the BGB (see simplified geological map in Figs. 1a–1c with U-Pb zircon constraints). Several early Archean mafic-ultramafic hydrothermal environments have been identified, particularly in the oldest part of the BGB stratigraphy related to the shallow subsurface hydrothermal activity (e.g., Hanor and Duhač 1990; Hoffman and Harris 2008). Retrograde alteration and sheet silicate formation have also been recorded in mafic-ultramafic tectonite zones (Grosch et al. 2009, 2012). Various metabasaltic and serpentinized ultramafic field

**TABLE 1.** List of samples and analytical technique

Sample ID	JB sample no.	Sample type	Mineralogy	HySpex imagery	ASD	RELAB	Emission
KV1	JB1570	rock slab	plagioclase, quartz	X	X		X
KV1	JB1571	coarse grains (~1 mm)	hornblende and		X	X	X
KV1	JB1572	powder (~<125 µm)	chlorite		X		X
THS-4		rock slab	chlorite and	X			
THS-4	JB1573	coarse grains (~1 mm)	fuchsite mica		X	X	X
THS-4	JB1574	powder (~<125 µm)			X		X
KM-Dun		rock slab	serpentine and magnetite	X			
KM-Dun-b-01	JB1676	coarse grains (~1 mm)			X	X	X
KM-Dun-b-01	JB1677	powder (~<125 µm)			X		
KM-27	JB1678	coarse grains (~1 mm)	serpentine and chlorite		X	X	X
KM-27	JB1679	powder (~<125 µm)			X		
KM-spin-4	JB1680	coarse grains (~1 mm)	serpentine, magnetite		X	X	X
KM-spin-4	JB1681	powder (~<125 µm)	olivine		X		
KM-spin-18	JB1682	coarse grains (~1 mm)	serpentine, magnetite		X	X	X
KM-spin-18	JB1683	powder (~<125 µm)	olivine		X		
KMK-6		rock slab	serpentine, peridotite	X			
KD-pyrox		rock slab	serpentine	X			
KR1		rock slab	serpentine, chlorite	X			
KM-2C		rock slab	serpentine,	X			
HC3A		rock slab	chlorite, epidote, quartz	X			

outcrops of the Onverwacht Group are shown in Figures 1d–1h representing examples of a wide range of early Archean low-temperature hydrothermal settings on early Earth potentially useful as analog sites to martian environments.

Coarse-grained cumulate metaperidotites are commonly found in the BGB. These include ultramafic intrusions and mantle-derived rocks (Furnes et al. 2011; Grosch et al. 2012). An example of such rock types is the layered serpentized, olivine-rich meta-dunite of the 3.3 Ga Kromberg Formation of the mid-Onverwacht Group (see Fig. 1d). Other examples of serpentized peridotitic mantle rocks include the ultramafic meta-dunite complex of the 3.47 Ga upper Komati Formation (Dann 2000). Metadunites and metaperidotites are considered in this study as analogs for coarse-grained ultramafic cumulate rocks or mantle-derived rocks on Mars. The Onverwacht Group largely consists of tholeiitic metabasalt flows and pillow lavas. Pillow lava metabasalts of the 3.53 billion year old Theespruit Formation have been metamorphosed to upper greenschist/amphibolite facies conditions and are moderately deformed (Fig. 1f). These pillow metabasalts also have mica and amphibole as part of their metamorphic assemblage. Other oceanic pillow lava flows in the structurally overlying 3.47 Ga Hooggenoeg Formation and 3.3 Ga Kromberg Formation are exceptionally well-preserved, recording early seafloor magmatic and hydrothermal conditions (Fig. 1e). Metamorphic alteration temperature conditions in these rocks could be as low as ca.  $T = 140$  °C (Grosch et al. 2012). Metabasaltic flows in the Hooggenoeg, Kromberg, and Mendon Formations also record evidence for low-temperature, ca. 80–150 °C, seafloor silicification beneath overlying oceanic sediments (Hanor and Duchač 1990; Hofmann and Harris 2008). Metabasaltic alteration environments on Mars similar to these silicified basalts would be acid-sulfate leaching by sulfate-rich groundwater brines at low-temperature conditions. Most of the metabasaltic flows in the BGB consist of chloritized basalts (Fig. 1e) and altered basaltic komatiites, possibly similar to hydrothermally produced crustal chlorite in the subsurface of Mars (see Ehlmann et al. 2011a). The typical major element bulk rock composition of a metabasalt from the BGB is provided in Table 2. This composition is compared to those of the martian metabasalts Chesterlake and Deadwood measured by

the Mars Exploration Rover (MER) Opportunity at Endeavour Crater (Squyres et al. 2012; cf. Table 1). A strong similarity in whole-rock metabasalt composition is observed between these rocks. For this reason, further investigation of the metabasalts and serpentinites from the BGB was undertaken with the goal of providing geochemical constraints on the formation environments for related metabasalts on Mars.

The BGB is also the site of ultramafic volcanic rocks known as komatiites (Viljoen and Viljoen 1969b), which are generally considered to represent hotter mantle conditions on the early Earth. These rocks can be spinifex-textured due to the presence of elongated olivine or pyroxene hopper crystals. Ultramafic komatiites can be olivine- or pyroxene-rich. An olivine-spinifex komatiite from the 3.48 Ga Komati Formation of the BGB is shown in Figure 1g. Komatiites are typically altered by silicification or serpentization. Serpentized komatiites and komatiitic basalts typically contain the alteration assemblage chlorite + antigorite + brucite. Other serpentine minerals can also be present such as chrysotile. We propose that serpentized komatiites from the BGB region may help understand serpentized ultramafic rocks exposed on Mars. Serpentine has been observed in mélange terrains with olivine and other phyllosilicates at Claritas Rise and Nili Fossae, in small outcrops of the central peaks, walls or ejecta of a few impact craters, and associated with olivine and Mg-carbonate in Noachian rocks underneath a Hesperian flow in northern Syrtis Major west of the Isidis impact basin (Ehlmann et al. 2010). Carbonate + quartz + fuchsite (Cr-rich mica) + chlorite alteration horizons (Fig. 1h) have also been identified in komatiites, basaltic komatiites, metagabbros, and metaperidotites (e.g., Hanor and Duchač 1990; Hofmann and Harris 2008; Grosch et al. 2012). These typically occur in retrograde tectonic shear zones (Grosch et al. 2012). Given the high CO<sub>2</sub> activity in martian groundwater brines (Michalski et al. 2013), these carbonate and sheet silicate BGB hydrothermal alteration sites may also prove to be useful analogs for altered olivine-bearing rocks on Mars such as those across the Nili Fossae region, in the flows of Syrtis Major, surrounding the Isidis impact basin, and associated with smaller craters (e.g., Hamilton and Christensen 2005; Mustard et al. 2005, 2009; Bishop et al. 2013; Michalski et al. 2019).

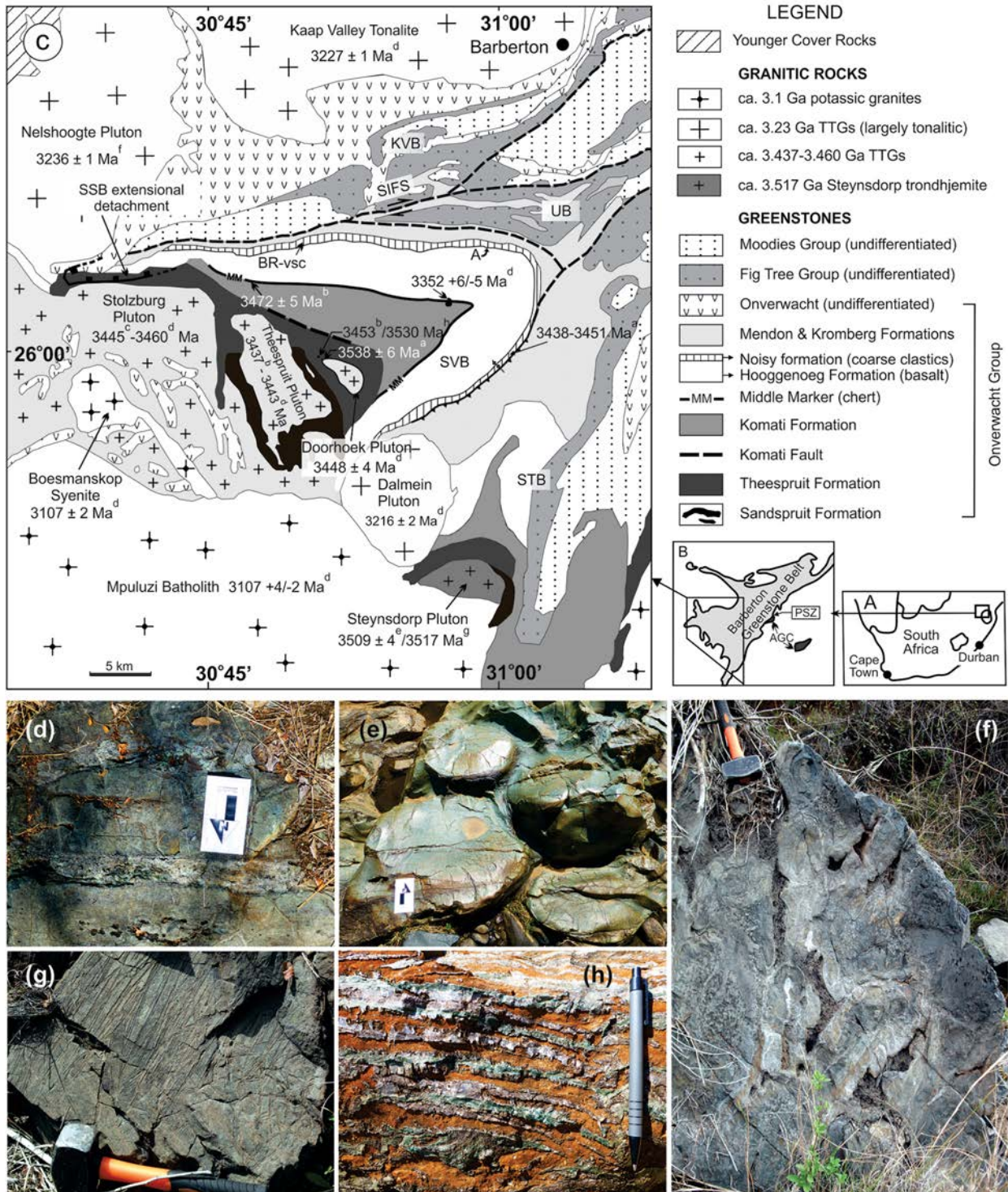


**FIGURE 1.** Simplified geological map of the Barberton greenstone belt (BGB). (a–b) Geographical location of the BGB on the boundary between South Africa and Swaziland. (c) Geological map with U-Pb age constraints of various rock types of the Onverwacht Group of the Barberton Supergroup (see Grosch et al. 2011 and references therein). (d–h) Various field outcrops showing altered serpentinized ultramafic rocks and metabasalts as potential analog sites for hydrothermal alteration of crust on Mars. (Color online.)

**TABLE 2.** Whole rock compositions in wt% element oxides of a typical BGB metabasalt compared to altered metabasalts on Mars

	Barberton BG-196 metabasalt (this study)	Mars <sup>a</sup> Chesterlake metabasalt	Mars <sup>a</sup> Deadwood metabasalt
SiO <sub>2</sub>	45.23	45.5	44
TiO <sub>2</sub>	1.04	1.09	0.98
Al <sub>2</sub> O <sub>3</sub>	12.18	8.8	8.3
FeO <sub>t</sub>	20.01	20.10	19.4
MnO	0.31	0.48	0.22
MgO	9.96	8.8	5.7
CaO	8.1	6.8	6.7
Na <sub>2</sub> O	0.68	2.7	2.2
K <sub>2</sub> O	0.81	0.41	0.62
P <sub>2</sub> O <sub>5</sub>	0.06	1	0.78
L.O.I.	2.2	na	na
Total	100.58	na	na

<sup>a</sup> Rock compositional data from Squyres et al. (2012).

## METHODS

### Sample preparation

A list of the 11 rock samples analyzed in this study is provided in Table 3. This includes the BGB rock formation where the sample was collected (see Map in Fig. 1) and the corresponding GPS coordinates. Multiple samples were prepared for each rock of interest in the rock preparation lab at the University of Bergen, Norway. For each hand specimen sample, a thin section (24 mm wide by 48 mm long and ca. 38 μm thick) was prepared for petrographic analysis and mineral identification (Grosch et al. 2012). Portions of each sample were crushed to prepare coarse-grained samples by using a jaw crusher, which produced rock chips approximately 0.3–0.8 mm in diameter. Additional samples were further pulverized into rock powers using a clean agate mill. Using a rock saw, rock slabs were cut for selected samples with dimensions of ca. 25 by 50 mm for the HySpex VNIR spectral scanning.

### Sample petrography

Photomicrographs of representative samples and associated alteration assemblages are shown in Figure 2. The metadunite sample (KM-dun) from the ca. 3.49 Ga upper Komati Formation displays a coarse-grained texture consisting mainly of subhedral olivine grains replaced by low-temperature serpentine alteration minerals (Fig. 2a). A two-stage alteration pattern is present with the cores of former olivine grains altered to fine-grained serpentine and magnetite that is, in turn, surrounded by outer rims of chlorite (clinochlore). Relic igneous phases could not be identified, and the sample displays a high degree of chloritization. The serpentinized spinifex komatiite sample (KM-spin18) consists of elongated, olivine hopper crystals as well as dendritic and plumose olivine crystal aggregates in the matrix between elongated spinifex blades (Fig. 2b). The olivine hopper crystals are extensively altered mainly to chlorite and magnetite with minor serpentine, whereas the finer-grained crystals in the matrix are largely replaced by serpentine. The altered komatiite sample (KM-2c) consists mainly of olivine replaced by brucite and antigorite (high-temperature serpentine), with a rim of carbonate (dolomite) and quartz (Fig. 2c). Antigorite veins in this sample display extensional cross-fibers (Fig. 2c).

The serpentinized ultramafic komatiite sample (KM-K6) contains olivine replaced by fine-grained antigorite and minor lizardite (low temperature serpentine), cross-cut by chlorite and lizardite veins (Fig. 2d). Magnetite, carbonate (dolomite),

and quartz are present with chlorite in the altered interstitial groundmass. The metabasaltic sample from the ca. 3.47 Ga Hooggenoeg Formation (HC3) features chloritized volcanic glass from a chilled pillow lava rim. The low-temperature alteration assemblage in this sample consists of green chlorite plus epidote, with accessory titanite and quartz (Fig. 2e). Sample HC3 contains the typical subgreenschist facies assemblage found in metabasalts from the BGB, although actinolitic amphibole is also frequently present in pillow lava metabasalts that have experienced greenschist facies conditions (Grosch et al. 2012). An extensively altered metabasalt from the ca. 3.55 Ga Theespruit Formation in the oldest part of the BGB (THS-4) consists mainly of coarse tabular grains of Cr-rich chlorite, magnetite, and sulfides (Fig. 2f). An altered felsic rock from the Kaap Valley Tonalite intrusion (KV1) is included as a control sample for comparison with the mafic-ultramafic rock types and enables the study of sericitized plagioclase and chloritized amphibole.

### Reflectance spectra of BGB samples

Reflectance spectra were acquired using two systems. VNIR spectra were measured from 0.35–2.5 μm under ambient conditions on rock surfaces, coarse-grained rock fragments, and rock powders (ground with a ball mill system to <125 μm) using an ASD FieldSpecPro spectrometer at the SETI Institute. Reflectance spectra were also measured on the particulate samples at RELAB at Brown University from 0.3 to 50 μm as in past studies (e.g., Bishop et al. 2008). The spectra are a composite of bidirectional spectra collected under ambient conditions at 5 nm spectral resolution from 0.3–1.3 μm relative to Halon and biconical FTIR spectra collected using a Nicolet spectrometer under a dehydrated environment (purged of H<sub>2</sub>O overnight) at 4 cm<sup>-1</sup> spectral resolution from 1–50 μm relative to a rough gold surface.

### Mid-IR emission spectra of BGB samples

Emissivity measurements were conducted in the Planetary Emissivity Laboratory (PEL) at the German Aerospace Center (DLR) in Berlin, Germany. Details on the laboratory setup, equipment, measurement methods, and calibration procedures can be found in Maturilli et al. (2019). To measure emissivity, samples were heated in two custom-designed external emissivity chambers, each of them attached to a Bruker Vertex80V FTIR spectrometer, and spectra were collected from ~630–4000 cm<sup>-1</sup> (or 2.5 to 16 μm) for these experiments. The samples were heated under purged air in an emissivity chamber attached to one of the FTIR spectrometers at PEL. Each sample was positioned in an aluminum cup and heated for one hour to reach the temperature steps of 20, 50, and 100 °C. The emissivity chamber walls were water-cooled to 5 °C during the sample measurements to minimize the spectral signature of the chamber measured at the detector. Successively, the same samples have been heated under vacuum in a second emissivity chamber, attached to another FTIR spectrometer. The whole optical path between the sample and the detector was under vacuum (0.7 mbar). A thermocouple was in contact with the sample surface to allow heating of the samples at the desired temperatures of 50 and 100 °C. All the samples measured in emissivity have been calibrated against an Acktar Fractal Black blackbody, measured under exactly the same conditions as the samples.

### Spectral imaging of rock slabs using HySpex

The rock slabs were scanned using the hyperspectral imaging spectrometer system (HySpex) at the GFZ Potsdam (Baarstad et al. 2005). The HySpex system uses two cameras: the VNIR 1600 covers the range 400–1000 nm and the 320m-e covers the range 1000–2500 nm. The samples are moved through the field of view of both cameras via a precision translation stage. This allows recording an image scene over the range 400–2500 nm. Both line scan cameras, the translation stage, and the light source (Hedler studio light with 1600 W) are mounted in a laboratory rack that

**TABLE 3.** List of samples in the study and their locations in the BGB stratigraphy

Acronym	Rock type/Mineralogy	Formation	Age (Ga)	S coordinates	E coordinates
THS-4	Greenschist facies pillow metabasite	Middle Theespruit Formation	3.53	25°59.854'	030°50.191'
KR1	Serpentinized komatiitic basalt	Lowermost Komati Formation	3.48	25°59.586'	030°51.094'
KM-2C	Serpentine veined komatiitic basalt	Lowermost Komati Formation	3.48	25°59.582'	030°51.098'
KMK-6	Serpentinized massive komatiite	Lower Komati Formation	3.48	25°59.557'	030°51.093'
KM-Spin 4	Serpentinized olivine spinifex komatiite	Lower Komati Formation	3.48	25°59.569'	030°51.088'
KM-Spin 18	Serpentinized olivine spinifex komatiite	Lower Komati Formation	3.48	25°59.319'	030°51.507'
KD-Pyrox	Altered pyroxene komatiite	Middle Komati Formation	3.48	25°59.264'	030°51.564'
KM-Dun-b	Serpentinized metadunite	Upper Komati Formation	3.48	25°58.912'	030°50.677'
KM-27	Serpentinized massive komatiite	Upper Komati Formation	3.48	25°58.837'	030°52.035'
HC3A	Greenschist facies thoeilitic basalt	Lower Hooggenoeg Formation	3.47	25°56.712'	030°53.064'
KV1	Altered felsic tonalite	TTG pluton	3.23	25°44.398'	030°59.902'

Notes: For further information on rock age see Grosch et al. (2011).

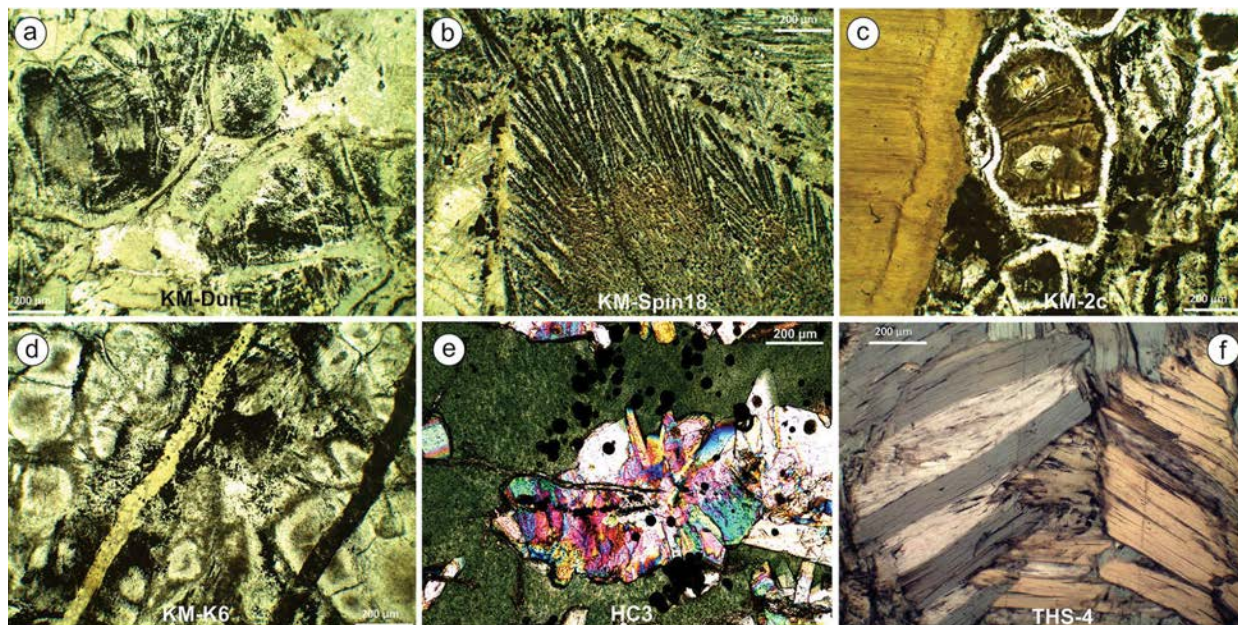


**FIGURE 2.** Petrographic images of relevant mafic and ultramafic rock types with associated low-temperature alteration assemblages (white scale bar is 200  $\mu\text{m}$ ). (a) KM-Dun = chloritized metadunite, (b) serpentinized olivine spinifex komatiite, (c) KM-2c = serpentinized komatiite with serpentine extensional veins (d) KM-K6 = serpentinized peridotitic komatiite with minor alteration veins (e) = HC3 chlorite-epidote-quartz assemblage in metabasaltic pillow lava chilled margin (f) altered komatiitic basalt with Cr-chlorite, serpentine and accessory opaques. (Color online.)

allows the use of different foreoptics and measurement distances for the HySpex cameras. For this study we selected lenses optimized for a distance of 30 cm above the sample. The geometric correction and reflectance retrieval are carried out with an in-house preprocessing chain that combines fast Fourier transform techniques (Xie et al. 2003) with scale invariant feature transformation (SIFT) techniques (Vedaldi and Fulkerson 2008) for image registration and a manual delineation of the reflectance panel for irradiance normalization and reflectance retrieval.

Automated mineral mapping from large imaging spectroscopy data sets was first proposed with the USGS Tetracorder (Clark 2003) and Material Identification and Characterization Algorithm (MICA) (Kokaly 2012) algorithms in an operational and scalable way. Both algorithms use spectral reference libraries and manual expert- and user-defined feature databases (Clark et al. 2007) to characterize surface material from an image spectroscopy data set. This work uses the EnMAP Geological Mapper (EnGeoMAP) in its second version (Mielke et al. 2016). The main difference to the aforementioned algorithms is the automated definition of characteristic absorption bands in both the unknown image spectroscopy data set and the reference library, assuming no a priori expert knowledge on the shape and position of the characteristic absorption features. The absorption band retrieval is carried out using the geometric hull absorption band retrieval algorithm (Mielke et al. 2015) via continuum removal (Clark et al. 1987).

## RESULTS

### VNIR and mid-IR spectral measurements on rock powders and fractions

VNIR reflectance spectra measured under ambient conditions from 0.35 to 2.5  $\mu\text{m}$  of the rock powders and coarse-grained material indicate the presence of alteration minerals (Fig. 3). Spectra of the KM-27 and KM-Dun samples (Fig. 3b) have features consistent with serpentine including strong, narrow bands at 1.39 and 2.33  $\mu\text{m}$  (e.g., King and Clark 1989; Bishop et al. 2008). Additional features due to serpentine are present in spectra of these samples near 1.91, 1.98, 2.11, and 2.45  $\mu\text{m}$  (Fig. 3d). Spectra of the KM-spin 4 and KM-spin 18 samples exhibit similar spectral features, although they are much weaker, indicating some

serpentine is present. Spectra of the THS-4 samples (Fig. 3a) have bands near 1.39, 1.91, 1.98, 2.11, 2.25, 2.32, and 2.38  $\mu\text{m}$  that are consistent with a mixture of Mg-rich chlorite and serpentine. Spectra of the KV1 samples (Fig. 3a) have bands near 1.41 and 2.21  $\mu\text{m}$  that are consistent with Al-OH in montmorillonite or mica, as well as a broad water band with a minimum at 1.91  $\mu\text{m}$  consistent with smectite minerals (e.g., Bishop et al. 2008). Variance in the shape of the Fe bands near 0.65–0.75, 0.88–0.93, and 1.03–1.13  $\mu\text{m}$ , the shape of the water band near 1.9–2.0  $\mu\text{m}$  and the position of the OH bands near 2.25–2.5  $\mu\text{m}$  are attributed to changes in the Fe/Mg-rich phyllosilicates. Spectra of several Fe/Mg-clays and olivine (forsterite) are included in Figure 3d for comparison.

VNIR spectra of the coarse-grained samples measured under a H<sub>2</sub>O-scrubbed environment from 0.3–4  $\mu\text{m}$  are shown in Figures 4a and 4c. These data show shifts in the OH and H<sub>2</sub>O stretching vibrations near 1.4, 1.9, 2.2–2.3, and 2.7–3  $\mu\text{m}$ . KV1 has features consistent with serpentine and quartz, while the THS-4 and KM-Dun-b spectra are darker and likely contain some basalt in addition to the chlorite and serpentine. The KM-27, KM-spin-4, and KM-spin-18 spectra are dominated by a downward slope characteristic of coatings or mixtures of grain size (e.g., Bishop 2019).

Mid-IR reflectance spectra of the coarse-grained samples are shown in Figures 4b and 4d. The reflectance features near 1000–1200  $\text{cm}^{-1}$  and from ~350–650  $\text{cm}^{-1}$  are characteristic of silicate minerals (e.g., Salisbury et al. 1991; Lane and Bishop 2019). The KV1 spectrum again appears to have the strongest spectral component due to quartz-based on features near 1100–1200  $\text{cm}^{-1}$  (Fig. 4b). The spectra of THS-4 and KM-Dun-b exhibit a basaltic type shape with additional features consistent

with chlorite (Fig. 4b). The KM-spin 4 spectrum contains features due to serpentine and chlorite near 1100, 1050, 870, 650, and 500–470  $\text{cm}^{-1}$ , while the KM-27 and KM-spin 18 spectra include features due to serpentine and chlorite but also contain a broader band near 950–1000  $\text{cm}^{-1}$  that could be due to forsteritic olivine and a shoulder near 550  $\text{cm}^{-1}$  consistent with magnetite (Fig. 4d).

Mid-IR emission spectra from ~600–1800  $\text{cm}^{-1}$  of the samples are presented in Figure 5. Four KV1 spectra were recorded for the slab, coarse grains, and powder (Fig. 5a). The KV1 slab spectrum includes some features consistent with a mixture of basalt and chlorite, but spectra of the particulate samples are

more consistent with a mixture containing quartz (Fig. 5b). The quartz grains in this sample are apparently more dominant in the particulate samples. Emission spectra of quartz include features due to Si-O stretching vibrations near 1100–1200  $\text{cm}^{-1}$  and bending vibrations near 500  $\text{cm}^{-1}$  (e.g., Wenrich and Christensen 1996; Christensen et al. 2000; Lane and Bishop 2019). Basalt emission spectra in this region exhibit a broader band in the silicate stretching region that has been important in modeling the spectra of Mars (e.g., Christensen et al. 2001). Spectra of plagioclase (albite) and hornblende are also shown for comparison as they were found in petrological analyses and could be present

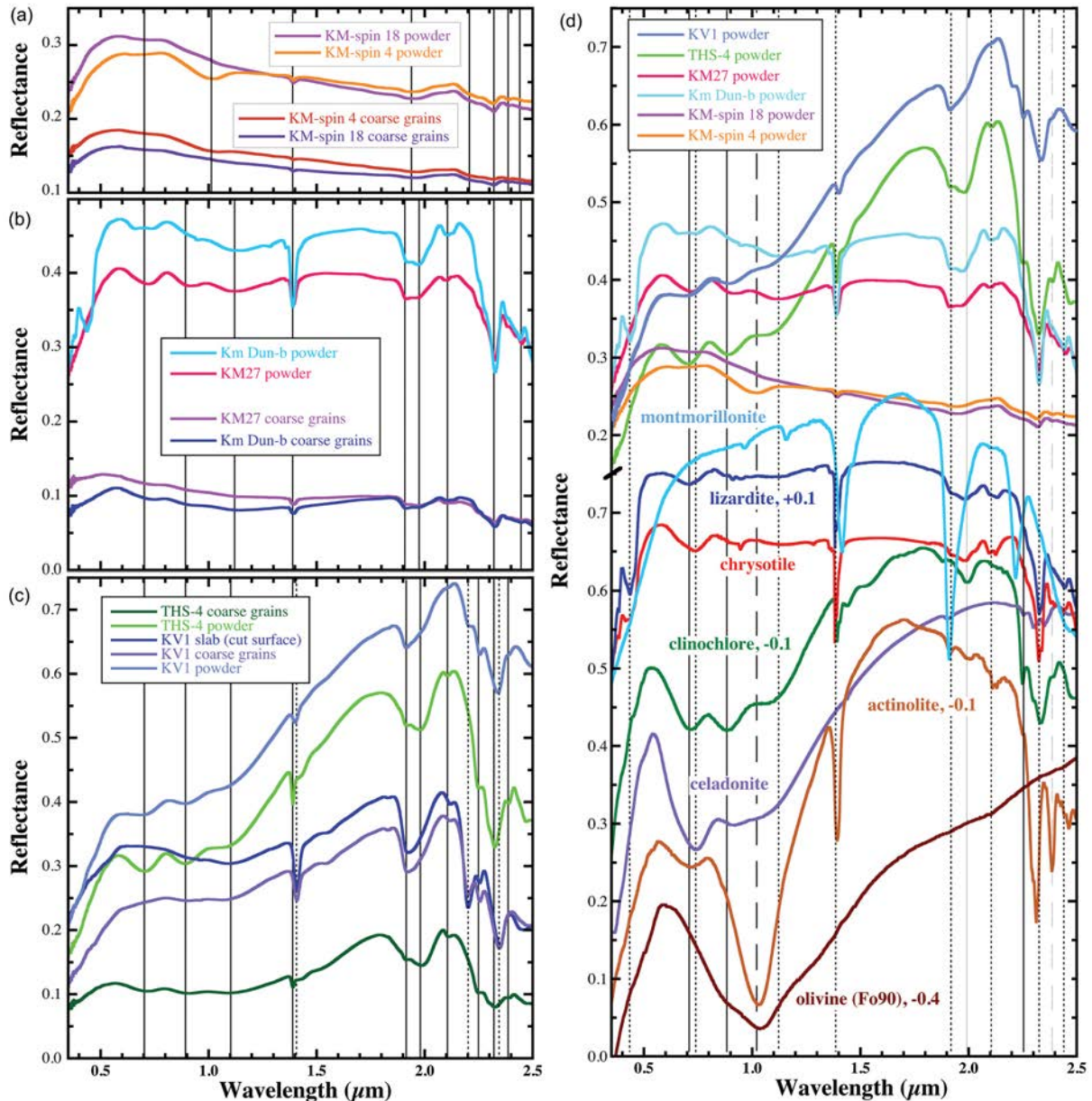


**FIGURE 3.** VNIR reflectance spectra from 0.35 to 2.5  $\mu\text{m}$  measured with the ASD spectrometer under ambient conditions. (a) KV1 and THS-4 spectra, (b) KM-27 and Km-Dun-b spectra, (c) KM-spin 4 and KM-spin 18 spectra, (d) fine-grained BGB samples compared with minerals from the Bishop library (e.g., Bishop 2019) and synthetic olivine (Fo90) from Isaacson et al. (2014). Spectral features due to electronic or vibrational absorptions are marked on the plots to facilitate comparison of the BGB samples with each other and their mineral components. (Color online.)

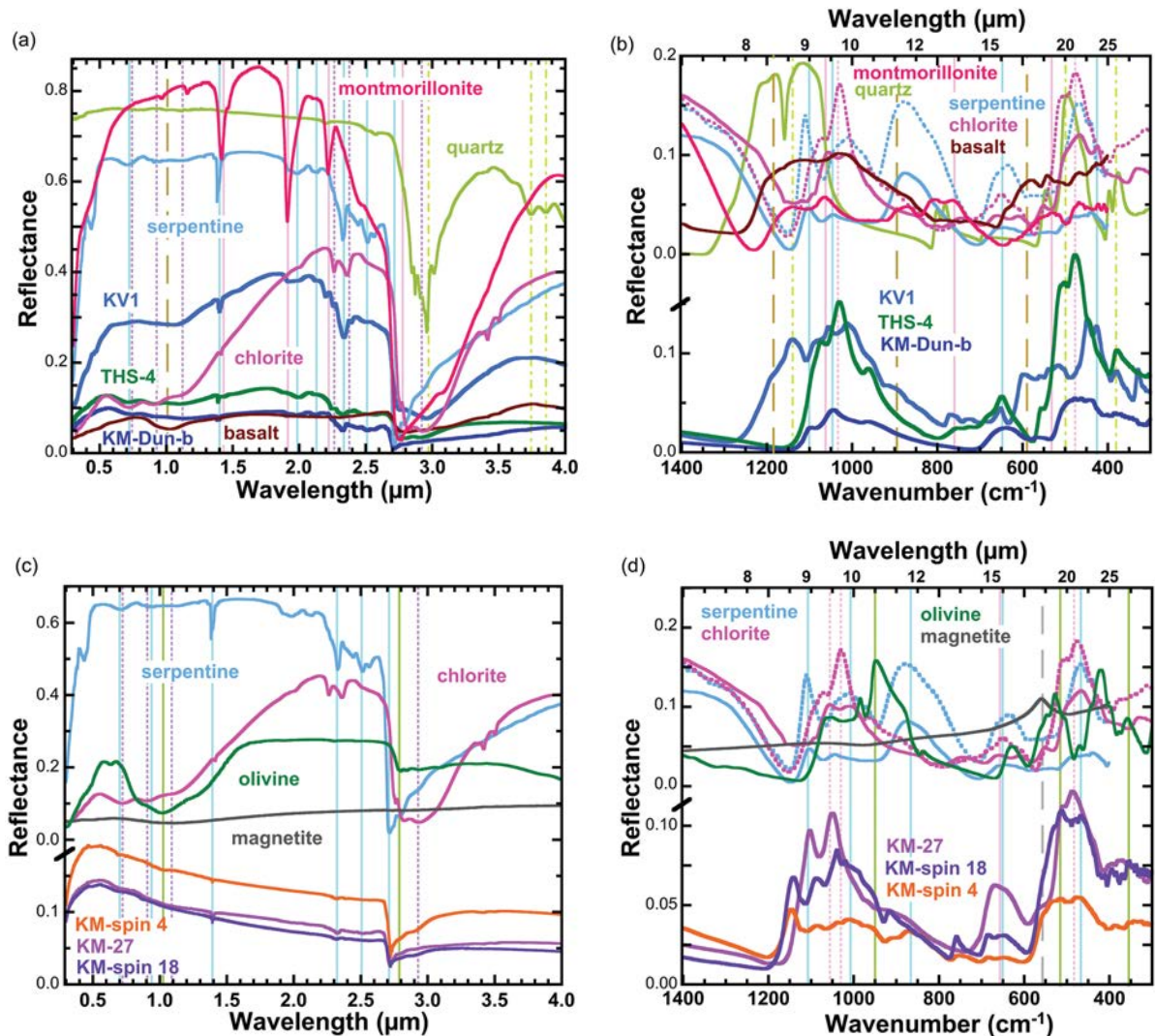


**FIGURE 4.** Reflectance spectra across the VNIR and mid-IR range measured under an H<sub>2</sub>O- and CO<sub>2</sub>-purged environment. Spectra of the coarse-grained samples KV1, THS-4, and ZKM-Dun-b are shown in **a** from 0.3–4 μm as a function of wavelength and **(b)** from 1400 to 300 cm<sup>-1</sup> as a function of wavenumber, while spectra of KM-27, KM-spin-4, and KM-spin-18 are shown in **c** and **d**. Reflectance spectra of basalt and selected minerals (Bishop 2019) are provided for comparison. Spectra of the clay minerals chamosite (Fe-rich chlorite, solid line), clinocllore (Mg-rich chlorite, dotted line), lizardite (serpentine, solid line), chrysotile (serpentine, dotted line), and montmorillonite SAZ-1 (Al-rich smectite) are from Bishop et al. (2008), and the basalt spectrum of sample G2 from Bishop et al. (2002) is described in Harloff and Arnold (2001). Vertical lines mark features due to minerals in the spectra. (Color online.)

at lower abundances based on the emission spectra. The THS-4 emission spectra are dominated by features due to the chlorite mineral chamosite (Fig. 5b), as also observed in the VNIR spectra. The chlorite-type bands near 950, 1030, and 1070 cm<sup>-1</sup> are observed in both grain sizes of this sample, although the water band near 1600 cm<sup>-1</sup> is more pronounced in the spectrum of the fine-grained sample, as expected. Emission spectra of KM-27 and KM-Dun-b (Fig. 5c) include features consistent with serpentine and chamosite, but also contain a broader emission feature spanning 900–1200 cm<sup>-1</sup> that is consistent with basalt. Emission spectra of KM-spin-4 and KM-spin-18 (Fig. 5d) are even more characteristic of basalt, but could have smaller components of serpentine or olivine, as found in the petrologic analyses.

### Spectral imaging of rock slabs

False color composite images of the rock slabs are shown in Figures 6a and 6b, and point spectra of locations marked on Figures 6a and 6b are shown in Figures 6f and 6g together with mineral reference spectra from the U.S. Geological Survey (USGS) digital spectral library (Clark et al. 2007). The extracted characteristic absorption bands of the unknown image pixel spectrum and the reference library standards are compared via a weighted fitting technique similar to the TetraRecorder (Clark 2003) and MICA (Kokaly 2012) algorithms. Figures 6c, 6d, and 6e show a best-weighted fit material map using sensor specific thresholds, which are lower than the user-defined threshold values considering the high signal-

to-noise performance (SNR) of the HySpex system (Baarstad et al. 2005).

Samples such as KMK-6 and KR1 are too dark (low overall albedo) to be analyzed with reflectance values below the dark cellular-rubber background, as shown in Figure 6f. The hyperspectral scanning of the samples indicates the presence of clay minerals, in particular chlorite and serpentine. The reflectance spectra of samples KM-Dun and THS-4 indicate the presence of both chlorite and serpentine, consistent with the petrographic identification from thin-section microscopy (see Fig. 2). VNIR spectral imaging of sample KM-2c revealed the presence of antigorite veins, also consistent with the petrographic observations (Fig. 2c). Collectively, the HySpex VNIR imaging method tested here succeeded in mapping chlorite and serpentine clay mineralogy identified in our samples through petrographic thin-section analyses, bulk VNIR, and mid-IR spectral measurements.

Spectra of a few surface spots from the HySpex imaging spectrometer are compared with bulk spectra of the crushed samples in Figure 7. These data illustrate how the bulk spectra contain features present in one or two spot spectra that are focused on individual mineral grains in the rock. For example,

the surface spot measured on rock slab KM 2C contains features due to chlorite that are also found in the spectra of the THS-4 bulk grains sample. The HC3A surface spot spectrum contains a broad Fe band near 0.9–1.2  $\mu\text{m}$  that is consistent with olivine, bands near 2.0, 2.25, and 2.35  $\mu\text{m}$  that are consistent with chamosite, and a band at 2.20  $\mu\text{m}$  due to Al-OH in phyllosilicates. Spectra of the KV1 surface spot and KV1 bulk grains also contain phyllosilicate OH features from 2.2 to 2.35  $\mu\text{m}$ , but show variations in the abundance of the chamosite and Al-smectite. The KM-Dun spectra exhibit basalt-type signatures and the basalt band is more clearly defined in the surface spot spectrum. A small shift in the wavelength of the OH combination band near 2.33–2.35  $\mu\text{m}$  represents changes in the Fe/Mg abundance in the chlorite measured by each technique.

## DISCUSSION

Based on orbital data, a very wide range of aqueous environments of Noachian age has been recognized on Mars, and their occurrence implies that hydrothermal sub-surface alteration of mafic-ultramafic rocks was widespread during the Noachian Period on ancient Mars (Wray et al. 2009; Bishop et al. 2013,

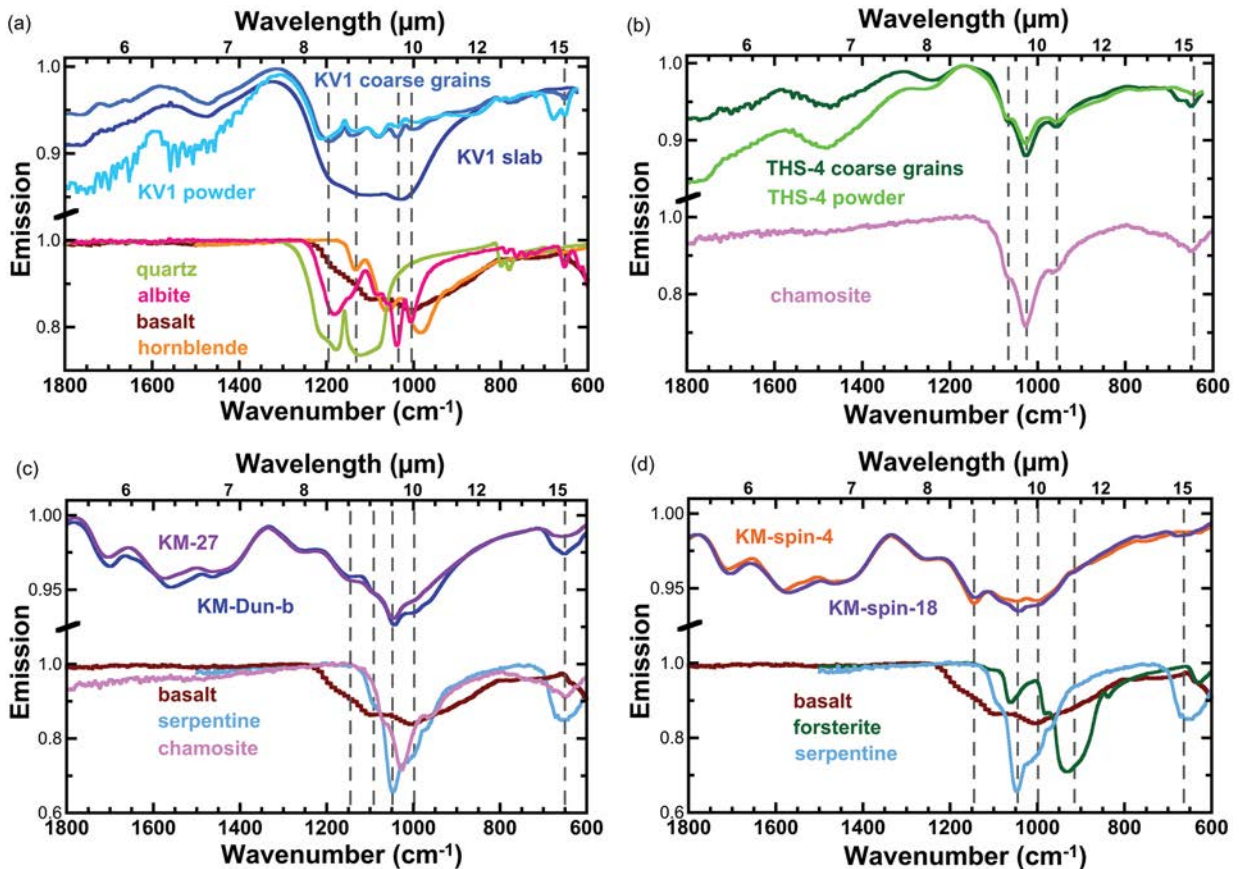


**FIGURE 5.** Mid-IR emission spectra of BGB samples (a) KV1, (b) THS-4, (c) KM-Dun-b and KM-27, and (d) KM-spin-4 and KM-spin-18. Spectra are shown for multiple sample textures for samples KV1 and THS-4 to illustrate the influence of grain size and surface type on the spectra. Emission spectra of selected minerals and basalt are shown for comparison. Emission spectra of the chamosite (Fe-rich chlorite) is from Bishop et al. (2008), the basalt spectrum is sample G2 from Bishop et al. (2002) that is described in Harloff and Arnold (2001), the serpentine, hornblende, and forsterite are from Lane and Bishop (2019), and the quartz and albite spectra are from the ASU library (Christensen et al. 2000). Vertical lines mark features in the BGB spectra associated with the rock and mineral spectra. (Color online.)

2018). It is likely that some of the low-temperature clay minerals observed on Mars are due to hydrothermal processes, particularly those associated with large impact craters. Smectite, kaolinite, and illite are common clay minerals on Mars that form at low temperatures below  $\sim 100$  °C. However, moderate to higher temperature clay minerals ( $\sim 100$ – $400$  °C) such as serpentine, chlorite, and talc have been confirmed in Leighton Crater and other sites using hyperspectral analysis in crater ejecta, knobby terrains, or as part of discontinuous layers in craters or valley walls of the Nili Fossae region (Amador et al. 2018; Brown et al. 2020). Furthermore, olivine (precursor to serpentine) fractured rock units have been identified in deep regions of craters in the Nili Fossae region (e.g., Bramble et al. 2017) of similar age to early Archean rocks on Earth and serpentine has commonly been found as a possible higher temperature mineral in other regions of Mars (e.g., Ehlmann et al. 2010). Amador et al. (2018) have argued that serpentinization processes were pervasive in the early part of Mars' history as it was more geologically active then. Hence, early Earth and early Mars may have had similar

serpentinization processes in their early geological histories.

Even though not all alteration processes would have been the same on early Earth and Mars, the current study proposes that some subsurface mafic-ultramafic hydrothermal environments on ancient Mars and early Archean Earth may have been similar. In this context, the rock sequences of the Paleoproterozoic Barberton greenstone belt of South Africa provide unique martian analogs as these rocks are exceptionally well-preserved and record early Earth (and perhaps martian-type) subsurface hydrothermal/alteration processes. In situ exploration by rovers, remote sensing studies, and meteorite evidence has indicated the presence of altered gabbros, olivine-/pyroxene-bearing metabasalts, and possible serpentinites on Mars (e.g., Ehlmann and Edwards 2014; Ruff et al. 2019; Hamilton et al. 2019; Murchie et al. 2019; McSween 2015). We present selected 3.5 to 3.3 billion year old Archean greenstone belt analog samples that include altered tholeiitic metabasalts and serpentinized ultramafic rocks. Spectroscopic measurements were conducted on different scales, namely bulk analyses on rock fragments and rock powders and

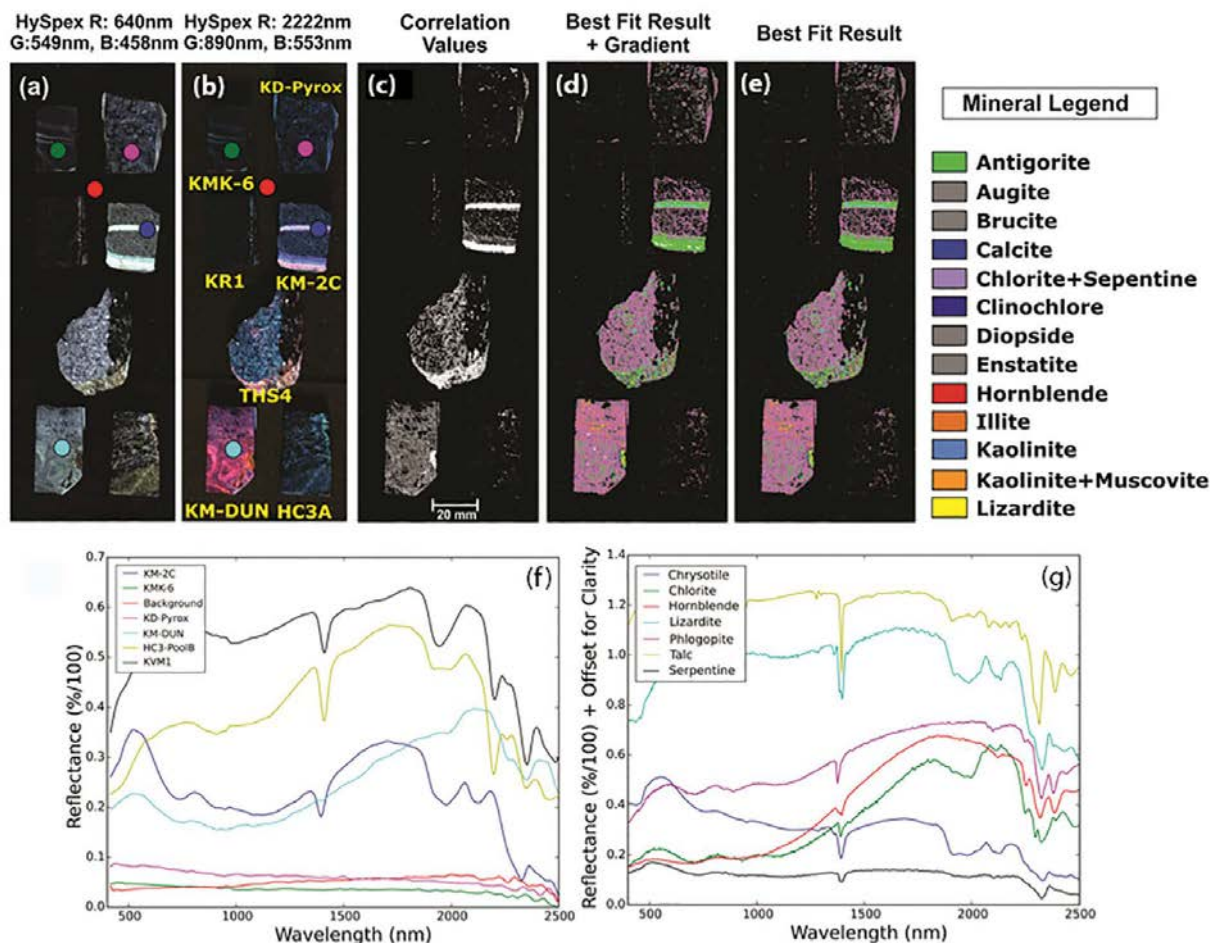


**FIGURE 6.** VNIR spectral imaging of rock slabs KMK-6, KD-Pyrox, KR1, KM-2C, THS4, KM-DUN, and HC3A. (a) Color maps of the rock slabs using R: 640 nm, G: 549 nm, B: 458 nm; (b) color maps of the rock slabs using R: 2222 nm, G: 890 nm, B: 553 nm; (c) maps of correlation values; (d) maps of the best fit plus gradient; (e) maps of the best fit; (f) VNIR spectra collected from regions on the rock slabs marked in a and b that were selected to highlight the observed clay mineralogy in the samples; and (g) lab spectra of minerals from the USGS spectral library for comparison. (Color online.)

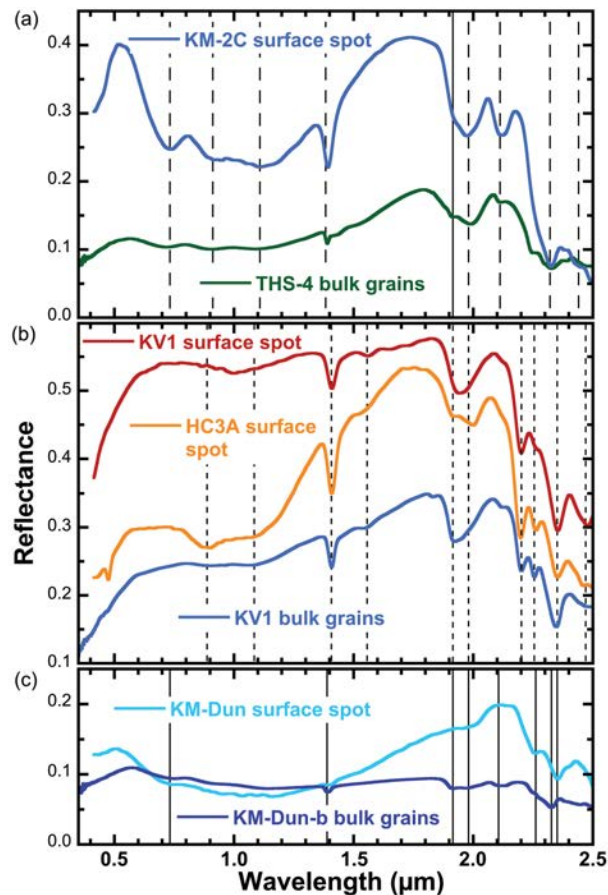


**FIGURE 7.** Spectra of a few surface spots from the HySpex imaging spectrometer compared in the same diagram with bulk spectra of the selected crushed samples. (Color online.)

microscale analyses on rock slabs by HySpex in situ analysis. VNIR reflectance, mid-IR emission, and VNIR spectral imaging have successfully identified serpentine and chlorite alteration mineralogy irrespective of scale or material form. The petrography and mineralogy of the samples were analyzed in terms of relic igneous phases and clay mineral alteration and are in good agreement with spectral identification of minerals in the samples. We expanded past studies by acquiring VNIR reflectance and mid-IR emission spectra on these early Archean samples for comparison with orbital spectral data of Mars.

The HySpex instrument hyperspectral data used to “map” the mineralogy of the rock samples have proven to be useful in mineral identification, and the results compare well with bulk spectroscopic analyses. This technique has the potential to provide useful information for both terrestrial studies and studies seeking to understand hydrothermal alteration of rocks from current or future Mars missions. The power of imaging spectroscopy is that it coordinates textural and spatial information with mineralogy, information that is not gained from bulk analysis of rock powders or rock chips. This spatial and textural-related data are needed to demonstrate that a clay-bearing deposit on Mars may be hydrothermal in origin and also that a terrestrial

deposit may indeed be a useful Mars analog. These kinds of analyses will be particularly useful in preparing for the micro-mega analyses to be collected by the ExoMars rover (Bibring et al. 2017). The relationships between alteration phases, primary igneous minerals, and textural characteristics are critical for piecing together the process history of metamorphosed terrestrial and extraterrestrial mafic and ultramafic rocks. In theory, in situ imaging spectroscopy of relevant rock surfaces has the power to aid in this type of direct comparative study. A HySpex-type instrument such as micromega attached to a Mars rover could also provide useful in situ scans of rock texture, mineralogy, and the alteration processes producing clay minerals.

## IMPLICATIONS

The Archean Barberton greenstone belt rocks hold significant potential for future petrological analog studies for Mars. Remote sensing hyperspectral studies on Mars have revealed evidence for hydrothermal activity involving not only chloritization, but also carbonate formation in altered mafic-ultramafic rocks (e.g., Viviano et al. 2013; Ehlmann and Edwards 2014; Lane and Christensen 1997; Hamilton et al. 2019; Brown et al. 2020), sulfates (Bishop et al. 2013), and hematite on Mars (Christensen et al. 2000, 2001; Lane et al. 2002). Several early Archean rocks from the Barberton greenstone belt could serve as hyperspectral petrological analogs for martian environments in future analog studies: banded iron formations for hematite and magnetite layers; hydrothermal and sedimentary barite units for sulfate analogs; as well as carbonitized and silicified mafic-ultramafic rocks for siderite, dolomite, and calcite hyperspectral studies. Silicified metabasalts and serpentinites of the Barberton greenstone belt may also contribute to understanding acid leaching processes on Mars (cf. Yant et al. 2016). The upcoming Mars2020 rover analyses of Jezero crater will investigate phyllosilicate and carbonate-bearing outcrops in  $\delta$  sediments, as well as basaltic bedrock containing olivine, chlorite, and serpentine (e.g., Goudge et al. 2017; Bramble et al. 2017; Amador et al. 2018; Brown et al. 2020). If chlorite- and serpentine-bearing rocks are encountered by Mars2020, the rock textures and spectral analyses in this study will provide ground truth for understanding the potential formation conditions for those rocks.

## ACKNOWLEDGMENTS

The authors are grateful for the assistance of T. Hiroi in measuring reflectance spectra at the NASA-supported RELAB facility at Brown University and to M. Lane for helpful comments during review. The authors also appreciate the use of mineral spectra from the Arizona State University (ASU) Mars Space Flight Facility: <https://speclib.asu.edu/>, and the U.S. Geological Survey (USGS) spectroscopy lab: <https://www.usgs.gov/labs/spec-lab/capabilities/spectral-library>. Rhodes University Research Office is acknowledged for partial financial support.

## REFERENCES CITED

- Amador, E.S., Bandfield, J.L., and Thomas, N.H. (2018) A search for minerals associated with serpentinization across Mars using CRISM spectral data. *Icarus*, 311, 113–134.
- Baarstad, I., Løke, T., and Kaspersen, P. (2005) ASI—A new airborne hyperspectral imager. In Proceedings of the 4th EARSeL Workshop on Imaging Spectroscopy—New Quality in Environmental Studies. Warsaw, Poland.
- Banerjee, N.R., Simonetti, A., Fumes, H., Staudigel, H., Muehlenbachs, K., Heaman, L., and Van Kranendonk, M.J. (2007) Direct dating of Archean microbial ichnofossils. *Geology*, 35, 487–490.
- Bibring, J.-P., Hamm, V., Pilorget, C., Vago, J.L., and MicrOmega Team (2017) The MicrOmega Investigation Onboard ExoMars. *Astrobiology*, 17, 621–626.
- Bishop, J.L. (2019) Visible and near-infrared reflectance spectroscopy of geologic materials. In J.L. Bishop, J.F. Bell III, and J.E. Moersch, Eds., *Remote Compo-*

- sitional Analysis: Techniques for Understanding Spectroscopy, Mineralogy, and Geochemistry of Planetary Surfaces, p. 68–101. Cambridge University Press.
- Bishop, J.L., Schiffman P., and Southard R.J. (2002) Geochemical and mineralogical analyses of palagonitic tuffs and altered rinds of pillow lavas on Iceland and applications to Mars. In J.L. Smellie and M.G. Chapman, Eds., *Volcano-ice interactions on Earth and Mars*, 371–392. Geological Society, Special Publication No. 202, London.
- Bishop, J.L., Murad, E., Lane, M.D., and Mancinelli, R.L. (2004) Multiple techniques for mineral identification on Mars: A study of hydrothermal rocks as potential analogues for astrobiology sites on Mars. *Icarus*, 169, 331–323.
- Bishop, J.L., Schiffman, P., Murad, E., Dyar, M.D., Drief, A., and Lane, M.D. (2007) Characterization of alteration products in Tephra from Haleakala, Maui: A visible-infrared spectroscopy, Mössbauer spectroscopy, XRD, EPMA and TEM study. *Clays and Clay Minerals*, 55, 1–17.
- Bishop, J.L., Lane, M.D., Dyar, M.D., and Brown, A.J. (2008) Reflectance and emission spectroscopy study of four groups of phyllosilicates: Smectites, kaolinite-serpentines, chlorites and micas. *Clay Minerals*, 43, 35–54.
- Bishop, J.L., Tirsch, D., Tornabene, L.L., Jaumann, R., McEwen, A.S., McGuire, P.C., Ody, A., Poulet, F., Clark, R.N., Parente, M., and others (2013) Mineralogy and morphology of geological units at Libya Montes, Mars: ancient aqueously derived outcrops, mafic flows, fluvial features, and impacts. *Journal of Geophysical Research: Planets*, 118, 487–513.
- Bishop, J.L., Fairén, A.G., Michalski, J.R., Gago-Duport, L., Baker, L.L., Velbel, M.A., Gross, C., and Rampe, E.B. (2018) Surface clay formation during short-term warmer and wetter conditions on a largely cold ancient Mars. *Nature Astronomy*, 2, 206–213.
- Bost, N., Westall, F., Ramboz, C., Fouchera, F., Pullan, D., Meunier, A., Petit, S., Fleischer, I., Klingelhöfer, G., and Vago, J.L. (2013) Missions to Mars: Characterisation of Mars analogue rocks for the International Space Analogue Rockstore (ISAR). *Planet and Space Science*, 82–83, 113–127.
- Bramble, M.S., Mustard, J.F., and Salvatore, M.R. (2017) The geological history of Northeast Syrtis Major, Mars. *Icarus*, 293, 66–93.
- Bridges, J.C., Schwenzer, S.P., Leveille, R., Westall, F., Wiens, R.C., Mangold, N., Bristow, T., Edwards, P., and Berger, G. (2015) Diagenesis and clay mineral formation at Gale Crater, Mars. *Journal of Geophysical Research: Planets*, 120, 1–19.
- Bristow, T.F., Bish, D.L., Vaniman, D.T., Morris, R.V., Blake, D.F., Grotzinger, J.P., Rampe, E.B., Crisp, J.A., Achilles, C.N., Ming, D.W., and others (2015) The origin and implications of clay minerals from Yellowknife Bay, Gale crater, Mars. *American Mineralogist*, 100, 824–836.
- Brown, A.J., Walter, M.R., and Cudahy, T.J. (2004) Short-wave infrared reflectance investigation of sites of paleobiological interest: Applications for Mars exploration. *Astrobiology*, 4(3), 359–376.
- (2007) Hyperspectral imaging spectroscopy of a Mars analogue environment at the North Pole Dome, Pilbara Craton, Western Australia. *Australian Journal of Earth Sciences*, 52 (3), 353–364.
- Brown, A.J., Viviano C.E., and Goudge T.A. (2020) Olivine-carbonate mineralogy of the Jezero Crater Region. *Journal of Geophysical Research: Planets*, 125, e2019JE006011.
- Carter, J., Poulet, F., Bibring, J.P., Mangold, N., and Murchie, S. (2013) Hydrous minerals on Mars as seen by the CRISM and OMEGA imaging spectrometers: Updated global view. *Journal of Geophysical Research: Planets*, 118(4), 831–858.
- Christensen, P.R., Bandfield, J.L., Hamilton, V.E., Lane, M.D., Piatek, J.L., Ruff, S.W., and Stefanov, W.L. (2000) A thermal emission spectral library of rock-forming minerals. *Journal of Geophysical Research*, 105, 9735–9739.
- Christensen, P.R., Bandfield, J.L., Hamilton, V.E., Ruff, S.W., Kieffer, H.H., Titus, T.N., Malin, M.C., Morris, R.V., Lane, M.D., Clark, R.L., and others (2001) Mars Global Surveyor Thermal Emission Spectrometer experiment: Investigation description and surface science results. *Journal of Geophysical Research*, 106(E10), 23,823–23,871.
- Christensen, P.R., Mehall, G.L., Silverman, S.H., Anwar, S., Cannon, G., Gorelick, N., Kheen, R., Tourville, T., Bates, D., Ferry, S. and Fortuna, T. (2003) Miniature thermal emission spectrometer for the Mars exploration rovers, *Journal of Geophysical Research*, 108(E12), 8064.
- Clark, R.N. (2003) Imaging spectroscopy: Earth and planetary remote sensing with the USGS Tetracorder and expert systems. *Journal of Geophysical Research*, 108 (E12).
- Clark, R.N., King, T.V.V., and Gorelick, N. (1987) Automatic continuum analysis of reflectance spectra. *JPL Proceedings of the 3rd Airborne Imaging Spectrometer Data Analysis Workshop*, 138–142.
- Clark, R.N., Swayze, G.A., Wise, R., Livo, E., Hoefen, T.M., Kokaly, R.F., and Sutley, S.J. (2007) USGS digital spectral library splib06a. U.S. Geological Survey Data Series 2312. U.S. Geological Survey.
- Cockell, C.S. (2006) The origin and emergence of life under impact bombardment. *Philosophical Transactions of the Royal Society of London. Series B, Biological Sciences*, 361, 1845–1856.
- Craddock, R.A., and Howard A.D. (2002) The case for rainfall on a warm, wet early Mars. *Journal of Geophysical Research: Planets*, 107, 21–1–21–36.
- Cuadros, J., Michalski, J.R., Dekov, V., Bishop, J., Fiore, S., and Dyar, M.D. (2013) Crystal-chemistry of interstratified Mg/Fe-clay minerals from seafloor hydrothermal sites. *Chemical Geology*, 360–361, 142–158.
- Dann, J.C. (2000) The 3.5 Ga Komati Formation, Barberton Greenstone Belt, South Africa, Part I: New maps and magmatic architecture. *South African Journal of Geology*, 103, 47–68.
- Drabon, N., Heubeck, C.E., and Lowe, D. (2019) Evolution of an Archean fan delta and its implications for the initiation of uplift and deformation in the Barberton greenstone belt, South Africa. *Journal of Sedimentary Research*, 89 (9), 849–874.
- Ehlmann, B.L., and Edwards, C.S. (2014) Mineralogy of the Martian Surface. *Annual Review of Earth and Planetary Sciences*, 42, 291–315.
- Ehlmann, B.L., Mustard, J.F., Swayze, G.A., Clark, R.N., Bishop, J.L., Poulet, F., Marais, D.J.D., Roach, L.H., Milliken, R.E., Wray, J.J., Barnouin-Jha, O., and Murchie, S.L. (2009) Identification of hydrated silicate minerals on Mars using MRO-CRISM: Geologic context near Nili Fossae and implications for aqueous alteration. *Journal of Geophysical Research*, 114 (E2). doi:10.1029/2009JE003339.
- Ehlmann, B.L., Mustard J.F., and Murchie S.L. (2010) Geologic setting of serpentine deposits on Mars. *Geophysical Research Letters*, 37(6), L06201. doi:10.1029/2010GL042596.
- Ehlmann, B.L., Mustard, J.F., Murchie, S.L., Bibring, J.P., Meunier, A., Fraeman, A.A., and Langevin, Y. (2011a) Subsurface water and clay mineral formation during the early history of Mars. *Nature*, 479, 53–60.
- Ehlmann, B.L., Mustard, J.F., Clark, R.N., Swayze, G.A., and Murchie, S.L. (2011b) Evidence for low-grade metamorphism, diagenesis, and hydrothermal alteration on Mars from phyllosilicate mineral assemblages. *Clays and Clay Minerals*, 59, 359–377.
- Ehlmann, B.L., Bish, D.L., Ruff, S.W., and Mustard, J.F. (2012) Mineralogy and chemistry of altered Icelandic basalts: Application to clay mineral detection and understanding aqueous environments on Mars. *Journal of Geophysical Research: Planets*, 117, no. E11.
- Ehlmann, B.L., Mustard, J.F., Murchie, S.L., Bibring, J.-P., Meunier, A., Fraeman, A.A., and Langevin, Y. (2013) Geochemical consequences of widespread clay mineral formation in Mars' ancient crust. *Space Science Reviews*, 174, 329–364.
- Fisk, M.R., Giovannoni, S.J., and Thorseth, I.H. (1998) Alteration of oceanic volcanic glass: textural evidence of microbial activity. *Science*, 281, 978–980.
- Furnes, H., Staudigel, H., Thorseth, I.H., Torsvik, T., Muehlenbachs, K., and Tummy, O. (2001) Bioalteration of basaltic glass in the oceanic crust. *Geochemistry, Geophysics, Geosystems* 2, GC000170.
- Furnes, H., Banerjee, N.R., Muehlenbachs, K., Staudigel, H., and de Wit, M.J. (2004) Early life recorded in Archean pillow lavas. *Science*, 304, 578–581.
- Furnes, H., de Wit, M.J., Robins, B., and Sandst ad, N.R. (2011) Volcanic evolution of the upper Onverwacht Suite, Barberton Greenstone Belt, South Africa. *Precambrian Research*, 186, 28–50.
- Goudge, T.A., Milliken, R.E., Head, J.W., Mustard, J.F., and Fassett, C.I. (2017) Sedimentological evidence for a deltaic origin of the western fan deposit in Jezero crater, Mars and implications for future exploration. *Earth and Planetary Science Letters*, 458, 357–365.
- Grosch, E.G., and Hazen, R.M. (2015) Microbes, mineral evolution, and the rise of microcontinents—Origin and coevolution of life with early Earth. *Astrobiology*, 15(10), 922–939.
- Grosch, E.G., and McLoughlin, N. (2014) Reassessing the biogenicity of Earth's oldest trace fossil with implications for biosignatures in the search for early life. *Proceedings of the National Academy of Sciences*, 111, 8380–8385.
- Grosch, E.G., McLoughlin, N., deWit, M.J., and Furnes, H. (2009) Deciphering Earth's deep history: drilling in Africa's oldest greenstone belt. *EOS Transactions, American Geophysical Union*, 90, 350–351.
- Grosch, E.G., Kosler, J., McLoughlin, N., Drost, K., Slama, J., and Pedersen, R.B. (2011) Paleorhean detrital zircon ages from the earliest tectonic basin in the Barberton Greenstone Belt, Kaapvaal craton, South Africa. *Precambrian Research*, 191, 85–99.
- Grosch, E.G., Vidal, O., Abu-Alam, T., and McLoughlin, N. (2012) PT-constraints on the metamorphic evolution of the Paleorhean Kromberg type-section, Barberton greenstone belt, South Africa. *Journal of Petrology*, 53, 513–545.
- Hamilton, V.E., and Christensen, P.R. (2005) Evidence for extensive, olivine-rich bedrock on Mars. *Geology*, 33, 433–436.
- Hamilton, V.E., Morris R.V., Gruener J.E., and Mertzman S.A. (2008) Visible, near-infrared, and middle infrared spectroscopy of altered basaltic tephra: Spectral signatures of phyllosilicates, sulfates, and other aqueous alteration products with application to the mineralogy of the Columbia Hills of Gusev Crater, Mars. *Journal of Geophysical Research: Planets*, 113(E12). doi: 10.1029/2007JE003049.
- Hamilton, V.E., Christensen, P.R., Bandfield, J.L., Rogers, A.D., Edwards, C.S., and Ruff, S.W. (2019) Thermal infrared spectral analyses of Mars from orbit using the Thermal Emission Spectrometer and Thermal Emission Imaging System. In J.L. Bishop, J.E. Moersch, and J.F. Bell III, Eds., *Remote compositional analysis: Techniques for Understanding Spectroscopy, Mineralogy, and Geochemistry of Planetary Surfaces*, p. 484–498. Cambridge University Press.
- Hanor, J.S., and Duchac, K.C. (1990) Isovolumetric silicification of early Archean komatiites: Geochemical mass balances and constraints on origin. *Journal of Geology*, 98, 863–877.
- Harloff, J., and Arnold, G. (2001) Near-infrared reflectance spectroscopy of bulk analog materials for planetary crust. *Planetary and Space Science*, 49(2), 191–211.
- Hofmann, A., and Harris, C. (2008) Stratiform alteration zones in Barberton Greenstone belt: A window into seafloor processes 3.5–3.3 Ga ago. *Chemical Geology*, 257, 224–242.
- Isaacson, P.J., Klima, R.L., Sunshine, J.M., Cheek, L.C., Pieters, C.M., Hiroi, T., Dyar, M.D., Lane, M.D., and Bishop, J.L. (2014) Visible to near-infrared optical properties of pure synthetic olivine across the olivine solid solution. *American Mineralogist*, 99, 467–478.

- Izawa, M., Banerjee, N.R., Shervais, J.W., Flemming, R.L., Hetherington, C.J., Muehlenbachs, K., Schultz, C., Das, D., and Hanan, B.B. (2019) Titanite mineralization of microbial bioalteration textures in Jurassic Volcanic Glass, Coast Range Ophiolite, California. *Frontiers in Earth Science*, 7, 315.
- King, T.V.V., and Clark, R.N. (1989) Spectral characteristics of chlorites and Mg-serpentines using high-resolution reflectance spectroscopy. *Journal of Geophysical Research*, 94, 13,997–14,008.
- Kokaly, R.F. (2012) Spectroscopic remote sensing for material identification, vegetation characterization, and mapping. In *Proceedings of the SPIE 8390, Algorithms and Technologies for Multispectral, Hyperspectral and Ultraspectral Imagery XVIII*; Baltimore Maryland, Volume 8390, pp. 839014.
- Lane, M.D., and Bishop J.L. (2019) Mid-infrared (thermal) emission and reflectance spectroscopy. In J.L. Bishop, J.F. Bell III, and J.E. Moersch, Eds., *Remote compositional analysis: Techniques for understanding spectroscopy, mineralogy, and geochemistry of planetary surfaces*, chapter 3, p. 42–67. Cambridge University Press.
- Lane, M.D., and Christensen, P.R. (1997) Thermal infrared emission spectroscopy of anhydrous carbonates. *Journal of Geophysical Research: Planets*, 102(E11), 25581–25592.
- Lane, M.D., Morris, R.V. Mertzman, S.A., and Christensen, P.R. (2002) Evidence for platy hematite grains in Sinus Meridiani, Mars. *Journal of Geophysical Research: Planets*, 107(E12).
- Lowe, D.R., Byerly, G.R., Kyte, F.T., Shukolyukov, A., Asaro, F., and Krull, A. (2003) Spherule beds 3.47–3.24 billion years old in the Barberton Greenstone Belt, South Africa: A record of large meteorite impacts and their influence on early crustal and biological evolution. *Astrobiology*, 3(1), 7–48.
- Lowe, D.R., Byerly, G.R., and Kyte, F.T. (2014) Recently discovered 3.42–3.23 Ga impact layers, Barberton Belt, South Africa: 3.8 Ga detrital zircons, Archean impact history, and tectonic implications. *Geology*, 42(9), 747–750.
- Marzo, G.A., Davila, A.F., Tornabene, L.L., Dohm, J.M., Fairén, A.G., Gross, C., Kneissl, T., Bishop, J.L., Roush, T.L., and McKay, C.P. (2010) Evidence for Hesperian impact-induced hydrothermalism on Mars. *Icarus*, 208, 667–683.
- Maturilli, A., Helbert, J., and Arnold, G. (2019) The newly improved set-up at the Planetary Spectroscopy Laboratory (PSL). *Proc. SPIE 11128, Infrared Remote Sensing and Instrumentation XXVIII* 11280T.
- McLoughlin, N., Grosch, E.G., Kilburn, M., and Wacey, D. (2012) Sulfur isotope evidence for a Paleoproterozoic subseafloor biosphere, Barberton, South Africa. *Geology*, 40, 1031–1034.
- McSween, H.Y. (2015) Petrology on Mars. *American Mineralogist*, 100, 2380–2395.
- Michalski, J.R., Kraft, M.D., Sharp, T.G., and Christensen, P.R. (2006) Effects of chemical weathering on infrared spectra of Columbia River Basalt and spectral interpretations of martian alteration. *Earth and Planetary Science Letters*, 248, 822–829.
- Michalski, J.R., Cuadros, J., Niles, P.B., Parnell, J., Rogers, A.D., and Wright, S.P. (2013) Groundwater activity on Mars and implications for a deep biosphere. *Nature Geoscience*, 6, 133–138.
- Michalski, J.R., Cuadros, J., Bishop, J.L., Darby Dyar, M., Dekov, V., and Fiore, S. (2015) Constraints on the crystal-chemistry of Fe/Mg-rich smectitic clays on Mars and links to global alteration trends. *Earth and Planetary Science Letters*, 427, 215–225.
- Michalski, J.R., Dobreá, E.Z.N., Niles, P.B., and Cuadros, J. (2017) Ancient hydrothermal seafloor deposits in Eridania basin on Mars. *Nature Communications*, 8, 15978.
- Michalski, J.R., Glotch, T.D., Rogers, A.D., Niles, P.B., Cuadros, J., Ashley, J.W., and Johnson, S.S. (2019) The geology and astrobiology of McLaughlin Crater, Mars: An ancient lacustrine basin containing turbidites, mudstones, and serpentinites. *Journal of Geophysical Research: Planets*, 124, 910–940.
- Mielke, C., Boesche, N.K., Rogass, C., Kaufmann, H., and Gauert, C. (2015) New geometric hull continuum removal algorithm for automatic absorption band detection from spectroscopic data. *Remote Sensing Letters*, 6, 97–105.
- Mielke, C., Rogass, C., Boesche, N., Segl, K., and Altenberger, U. (2016) EnGeoMAP 2.0—Automated hyperspectral mineral identification for the German EnGeoMAP Space Mission. *Remote Sensing*, 8(2), 127.
- Murchie, S.L., Bibring, J.P., Arvidson, R.E., Bishop, J.L., Carter, J., Ehlmann, B.L., Langevin, Y., Mustard, J.F., Poulet, F., Riu, L., Seelos, K.D., and Viviano, C.E. (2019) Visible to short-wave infrared spectral analyses of Mars from orbit using CRISM and OMEGA. In J.L. Bishop, J.E. Moersch, and J.F. Bell III, Eds., *Remote Compositional Analysis: Techniques for understanding spectroscopy, mineralogy, and geochemistry of planetary surfaces*, chapter 23, p. 453–483. Cambridge University Press.
- Mustard, J.F., and Tamas, J.D. (2017) Hydrogen production from the upper 15 km of martian crust via serpentinization: Implications for habitability. *Lunar and Planetary Science Conference. XLVIII*, The Woodlands, Texas, Abstract 2384.
- Mustard, J.F., Poulet, F., Gendrin, A., Bibring, J.-P., Langevin, Y., Gondet, B., Mangold, N., Bellucci, G., and Altieri, F. (2005) Olivine and pyroxene diversity in the crust of Mars. *Science*, 307, 1594–1597.
- Mustard, J.F., Ehlmann, B.L., Murchie, S.L., Poulet, F., Mangold, N., Head, J.W., Bibring, J.-P., and Roach, L.H. (2009) Composition, morphology, and stratigraphy of Noachian crust around the Isidis basin. *Journal of Geophysical Research*, 114 (E2), doi:10.1029/2009JE003349.
- Orcutt, B.N., Sylvan, J.B., Knab, N.J., and Edwards, K.J. (2011) Microbial ecology of the dark ocean above, at and below the seafloor. *Microbiology and Molecular Biology Reviews*, 75, 361–422.
- Oze, C., and Sharma, M. (2005) Have olivine, will gas: Serpentinization and the abiogenic production of methane on Mars. *Geophysical Research Letters*, 32(10), doi:10.1029/2005GL022691.
- Philippot, P., Van Kranendonk, M., Van Zuilen, Lepot, K., Rividi, N., Teitler, Y., Thomazo, C., Blanc-Valleron, M., Rouchy, J., Grosch, E.G., and de Wit, M.J. (2009) Drilling Archean hydrothermal and sedimentary settings of the Pilbara Craton, Western Australia and Barberton Belt, South Africa. *Comptes Rendus Palevol*, 8, 649–663.
- Ruff, S.W., Bandfield J.L., Christensen P.R., Glotch T.D., Hamilton V.E., and Rogers A.D. (2019) Thermal infrared remote sensing of Mars from rovers using the miniature thermal emission spectrometer. In J.L. Bishop, J.F. Bell III, and J.E. Moersch, Eds., *Remote compositional analysis: Techniques for understanding spectroscopy, mineralogy, and geochemistry of planetary surfaces*, Chapter 25, 499–512. Cambridge University Press.
- Salisbury, J.W., Walter, L.S., Vergo, N., and D’Aria, D.M. (1991) *Infrared (2.1–25 μm) Spectra of Minerals*, 267 p. Johns Hopkins University Press.
- Schiffman, P., Zierenberg, R.A., Marks, N., Bishop, J.L., and Dyar, M.D. (2006) Acid fog deposition at Kilauea Volcano: A possible mechanism for the formation of siliceous-sulfate rock coatings on Mars. *Geology*, 34, 921–924.
- Squyres, S.W., Arvidson, R.E., Bell, J.F. III, Calef, F. III, Clark, B.C., Cohen, B.A., Crumpler, L.A., de Souza, P.A. Jr., Farrand, W.H., Gellert, R., and others (2012) Ancient impact and aqueous processes at Endeavour Crater, Mars. *Science*, 336, 570–576.
- Staudigel, H., Furnes, H., McLoughlin, N., Banerjee, N.R., Connell, L.B., and Templeton, A. (2008) 3.5 billion years of glass bioalteration: Volcanic rocks as a basis for microbial life? *Earth Science Reviews*, 89(3–4), 156–176.
- Thorseth, I.H. (2011) Basalt (Glass, Endolith). In J. Reithner and V. Thiel, Eds., *Encyclopedia of Geobiology, Encyclopedia of Earth Sciences Series*, pp103–111. Springer-Verlag.
- Thorseth, I.H., Torsvik, T., Furnes, H., and Muehlenbachs, K. (1995) Microbes play an important role in the alteration of oceanic crust. *Chemical Geology*, 126, 137–146.
- Trowera, E.J., and Lowe, D.R. (2016) Sedimentology of the ~3.3 Ga upper Mendon Formation, Barberton Greenstone Belt, South Africa. *Precambrian Research*, 281, 473–494.
- Vedaldi, A., and Fulkerson, B. (2008) VLFeat: An open and portable library of computer vision algorithms. In *Proceedings of the 18th ACM international conference on Multimedia*, pp. 1469–1472.
- Viljoen, M.J., and Viljoen, R.P. (1969b) The geology and geochemistry of the lower ultramafic unit of the Onverwacht Group and a proposed new class of igneous rocks. *Geological Society of South Africa Special Publication*, 2, 55–86.
- Viviano, C.E., Moersch, J.E., and McSween, H.Y. (2013) Implications for early hydrothermal environments on Mars through the spectral evidence for carbonation and chloritization reactions in the Nili Fossae region. *Journal of Geophysical Research: Planets*, 118(9), 1858–1872.
- Walsh, M.W. (1992) Microfossils and possible microfossils from the Early Archean Onverwacht Group, Barberton Mountain Land, South Africa. *Precambrian Research*, 54(2–4), 271–293.
- Wenrich, M.L., and Christensen, P.R. (1996) Optical constants of minerals derived from emission spectroscopy: Application to quartz. *Journal of Geophysical Research*, 101, 15921–15931.
- Wray, J.J., Murchie, S.L., Squyres, S.W., Seelos, F.P., and Tornabene, L.L. (2009) Diverse aqueous environments on ancient Mars revealed in the southern highlands. *Geology*, 37(11), 1043–1046.
- Yant, M., Rogers, A.D., Nekvasil, H., Zhao, Y.Y.S., and Bristow, T. (2016) Spectral characterization of acid weathering products on Martian basaltic glass. *Journal of Geophysical Research: Planets*, 121(3), 516–541.
- Yant, M., Young, K.E., Rogers, A.D., McAdam, A.C., Bleacher, J.E., Bishop, J.L., and Mertzman, S.A. (2018) Visible, near-infrared and mid-infrared spectral characterization of Hawaiian fumarolic alteration near Kilauea’s December 1974 Flow: Implications for spectral discrimination of alteration environments on Mars. *American Mineralogist*, 103, 11–25.
- Xie, H., Hicks, N., Keller, G.R., Huang, H., and Kreinovich, V. (2003) An IDL/ENVI implementation of the FFT-based algorithm for automatic image registration. *Computers and Geoscience*, 29, 1045–1055.

MANUSCRIPT RECEIVED JUNE 8, 2020

MANUSCRIPT ACCEPTED AUGUST 26, 2020

MANUSCRIPT HANDLED BY PABLO SOBRON